



# Transition metal oxide window layer in thin film amorphous silicon solar cells



Liang Fang<sup>a</sup>, Seung Jae Baik<sup>b,\*</sup>, Koeng Su Lim<sup>c</sup>

<sup>a</sup> Department of Electrical Engineering, Tianjin Institute of Power Source, 6 Huakeqi Rd., Hi-tech Industrial Park, Tianjin 300384, China

<sup>b</sup> Department of Electrical, Electronic, and Control Engineering, Hankyong National University, 327 Jungang-ro, Anseong-si, Gyeonggi-do 456-749, Republic of Korea

<sup>c</sup> Department of Electrical Engineering, Korea Advanced Institute of Science and Technology (KAIST), 291 Daehak-ro, Daejeon 305-701, Republic of Korea

## ARTICLE INFO

### Article history:

Received 27 May 2013

Received in revised form 29 November 2013

Accepted 15 January 2014

Available online 22 January 2014

### Keywords:

Transition metal oxides

Amorphous silicon solar cells

Window layer

Thin film

## ABSTRACT

*Pin*-type hydrogenated amorphous silicon solar cells have been fabricated by replacing state of the art silicon based window layer with more transparent transition metal oxide (TMO) materials. Three kinds of TMOs: vanadium oxide, tungsten oxide, and molybdenum oxide ( $\text{MoO}_x$ ) were comparatively investigated to reveal the design principles of metal oxide window layers. It was found that  $\text{MoO}_x$  exhibited the best performance due to its higher work function property compared to other materials. In addition, the band alignment between  $\text{MoO}_x$  and amorphous Si controls the series resistance, which was verified through compositional variation of  $\text{MoO}_x$  thin films. The design principles of TMO window layer in amorphous Si solar cells are summarized as follows: A wide optical bandgap larger than 3.0 eV, a high work function larger than 5.2 eV, and a band alignment condition rendering efficient hole collection from amorphous Si absorber layer.

© 2014 Elsevier B.V. All rights reserved.

## 1. Introduction

Superstrate hydrogenated amorphous silicon (*a*-Si:H) solar cell, with an intrinsic layer sandwiched between *p*- and *n*-doped layers, is one of the main future options for cost-effective solar cells, which remains attractive in view of a variety of implementation in photovoltaic field [1,2]. Traditionally, a *p*-type window layer is essential to sustain built-in potential with rear *n* layer. Boron-doped amorphous silicon carbide (*p*-*a*-SiC) [3] and boron-doped microcrystalline silicon (*p*-*uc*-Si) [4] films were widely used as window layer of *a*-Si:H based solar cells. Recently, hydrogenated silicon oxide (*p*-*nc*-SiO<sub>x</sub>) has been studied [5]. However, the parasitic absorption and poor doping capability of *a*-Si:H based window layers restrict the overall device performance [6,7], and the design and improvement in the optical and electrical properties of the window layer in *pin*-type *a*-Si:H solar cells are necessary to further enhance conversion efficiency. Thermally evaporated transition metal oxides (TMOs) are promising to replace state of the art window layer materials due to wide optical bandgap ( $E_{opt}$ ), high work function (WF), and tunable *i*-*a*-Si:H/TMO interface. Furthermore, the process control is simpler than conventional plasma enhanced chemical vapor deposition. Recently, tungsten oxide ( $\text{WO}_x$ ) and molybdenum oxide ( $\text{MoO}_x$ ) have been demonstrated as window layer of *pin*-type *a*-Si:H based solar cells with performance enhancement compared to reference cells with *p*-*a*-SiC window layer [8,9]. In this paper, we investigate the design principles of TMO window layer in *a*-Si:H solar cells via comparative investigation of various TMO materials. In addition, the

influence of band alignment between TMO and amorphous absorber layer is investigated from compositional variation of TMO thin films.

## 2. Experiment

Asahi U-type glass (glass/SnO<sub>2</sub>) was used as substrate to deposit devices. Vanadium oxide ( $\text{V}_2\text{O}_x$ ),  $\text{WO}_x$ , and  $\text{MoO}_x$  films were deposited by a thermal evaporator under a vacuum of  $2.7 \times 10^{-4}$  Pa with  $\text{V}_2\text{O}_5$  source (Aldrich, 99.9%),  $\text{WO}_{2.9}$  source (Alfa Aesar, 99.99%) and  $\text{MoO}_3$  source (Alfa Aesar, 99.5%), respectively. The substrate temperature was kept constant at 20 °C. The thickness of the film was measured by an in situ quartz monitor, which is calibrated by spectroscopic ellipsometry (SE). A two-chamber system was used for fabricating *a*-Si:H solar cells, which consists of a photo-assisted chemical vapor deposition chamber for the *p*- and *n*-layers, an plasma enhanced chemical vapor deposition chamber for the intrinsic layer. The fabricated devices have a structure of glass/SnO<sub>2</sub>/TMO (10 nm)/*i*-*a*-Si (500 nm)/*n*-*a*-Si (40 nm)/Al, and the cell area was 0.092 cm<sup>2</sup>. 10-nm-thickness was the optimized thickness for the  $\text{MoO}_x$  window layer to realize best device performances, and additional scaling in  $\text{MoO}_x$  leads to a slight enhancement in photocurrent-generation with a degraded internal electric field [9]. These trends would be similar for other TMO materials, and the optimal thickness for each material can be different. However, we have compared the performances of different TCOs at a fixed thickness of 10 nm, which is the thickness condition in conventional *p*-*a*-SiC. To understand the essential criteria for TMO window layer and dependence of device performances on material properties, four kinds of substrates were prepared to fabricate devices: glass/SnO<sub>2</sub>, glass/SnO<sub>2</sub>/V<sub>2</sub>O<sub>x</sub>, glass/SnO<sub>2</sub>/WO<sub>x</sub>, and glass/SnO<sub>2</sub>/MoO<sub>x</sub>. All the samples have air exposure

\* Corresponding author. Tel.: +82 31 670 5325; fax: +82 31 670 5329.

E-mail address: [sjbaik@hknu.ac.kr](mailto:sjbaik@hknu.ac.kr) (S.J. Baik).

time around 1 min to control the influence of air contamination [10]. The detailed deposition conditions appeared in Ref. [11].

TMO films were grown on bare c-Si wafer for X-ray and ultraviolet photoemission spectroscopy (XPS, UPS) measurement, and on Corning 7059 glass for the  $\sigma_D$  and transmittance measurements. XPS and UPS study were performed using a Sigma probe system under an ultra high vacuum system ( $10^{-8}$  Pa) with Mg Ka X-ray source (1253.6 eV) and a He I (21.2 eV) discharge lamp. SE was performed to characterize the optical bandgap and refractive indices of the films (UVISEL, Jobin Yvon). Coplanar gap Al electrodes were deposited on the TMO films by a thermal evaporator to measure  $\sigma_D$  and active energy  $E_a$ , where the  $\sigma_D$  values were measured at different temperatures and the  $E_a$  was extracted from the slope of the Arrhenius plot. Photocurrent densities versus voltage ( $J$ - $V$ ) measurements were performed under AM 1.5, 100 mW/cm<sup>2</sup> irradiation using a Keithley 2400 source meter. A constant energy spectrophotometer (YQ-25-MV, JASCO) was used for external quantum efficiency (EQE) measurements.

### 3. Results and discussion

The photo  $J$ - $V$  characteristics of the devices with TMO window layers are shown in Fig. 1. For the devices (glass/SnO<sub>2</sub>/i/n/Al) without window layer the work function difference between SnO<sub>2</sub> and  $n$ - $a$ -Si (around 0.6–0.7 eV) produces internal electric field, and thus produces photovoltaic conversion with the efficiency around 3.0% with open circuit voltage ( $V_{oc}$ ) of 0.39 V and fill factor ( $FF$ ) of 0.61. Inserting a TMO window layer between the SnO<sub>2</sub> and intrinsic layer results in increased device parameters, and the differences in parameters have close relationship with the optical bandgap and electronic band alignment of

TMO films. For devices with WO<sub>x</sub> and MoO<sub>x</sub> window layer, the EQEs increase significantly at short wavelength region compared to other type of devices as shown in Fig. 1(b), which is consistent with the wide optical bandgap larger than 3.0 eV compared to that of V<sub>2</sub>O<sub>x</sub> based on the SE measurement, and the estimated bandgaps are 3.35, 3.25, and 2.3 eV for WO<sub>x</sub>, MoO<sub>x</sub>, and V<sub>2</sub>O<sub>x</sub>, respectively.

The  $V_{oc}$  of the solar cell without TMO layer is only 0.39 V, and increases to 0.42, 0.64 and 0.78 V for the cell with a 10-nm-thick V<sub>2</sub>O<sub>x</sub>, WO<sub>x</sub>, and MoO<sub>x</sub> window layer, respectively. One reason for the difference in  $V_{oc}$  is related to the WF of TMO materials. According to the UPS analyses, WF of V<sub>2</sub>O<sub>x</sub>, WO<sub>x</sub>, and MoO<sub>x</sub> was found to be 4.7, 4.9, and 5.35 eV, respectively. The other reason of the differences in  $V_{oc}$  is attributed to the carrier recombination at TMO/ $i$ - $a$ -Si interface, which implies the reduction of the electrons and holes quasi-Fermi level separation. The values of  $V_{oc}$  from the solar cell with V<sub>2</sub>O<sub>x</sub> and that with WO<sub>x</sub> show larger difference than that expected from the difference in WF. This implies that the V<sub>2</sub>O<sub>x</sub>/ $i$ - $a$ -Si interface contains larger interface state density than WO<sub>x</sub>/ $i$ - $a$ -Si interface in our interface forming condition (thermal evaporation at room temperature). The degradation of short wavelength EQE is related to the defect density near the window/ $i$ - $a$ -Si interface, because most of photo-generation occurs in this region. The additional reason of the small short wavelength EQE in the solar cell with V<sub>2</sub>O<sub>x</sub> shown in Fig. 1(b) may be due to a possible larger interface state density. Similarly, the device without window layer (glass/SnO<sub>2</sub>/i/n/Al) shows smaller EQE at 400 nm and smaller  $V_{oc}$  compared to those with WO<sub>x</sub> or MoO<sub>x</sub> window layers, which implies that the interface recombination at the SnO<sub>2</sub>/ $i$ - $a$ -Si interface significantly contributes to collection losses and narrowing the quasi-Fermi level separation.

The refractive indices of SnO<sub>2</sub>, WO<sub>x</sub>, and MoO<sub>x</sub> are measured to be almost constant in visible range with values around 2.0, 2.1, and 2.3, respectively. In addition, the refractive index of V<sub>2</sub>O<sub>x</sub> is reported to be in the range from 2.2 to 2.8 in the visible range [12]. These implies that the insertion of TMO's between SnO<sub>2</sub> and  $i$ - $a$ -Si:H can slightly reduce the optical reflectance, because the refractive index values of TMO's are between that of SnO<sub>2</sub> and that of  $i$ - $a$ -Si:H (around 4). This again confirms that the short wavelength EQE degradation in V<sub>2</sub>O<sub>x</sub> applied solar cells is due to the electronic effect, and slight differences with SnO<sub>2</sub>/ $i$ - $a$ -Si:H structure can be explained by the optical effect.

For materials as window layers of  $pin$ -type  $a$ -Si:H solar cells, an optical bandgap larger than 3.0 eV is necessary to realize near zero parasitic absorption (transparent to visible light) because only the photon energy  $h\nu > E_g$  can generate carrier (where  $h$  is the Planck's constant,  $\nu = c/\lambda$  with  $c$  the speed of light and  $\lambda$  the wavelength, and  $E_g$  is the energy gap of the window layer considered). At the same time, a high WF is essential to sustain high built-in potential and obtain a high  $V_{oc}$  as shown in the band diagram of Fig. 2. The photo-generated holes are collected via recombination processes at the  $i$ - $a$ -Si:H/TMO interface,

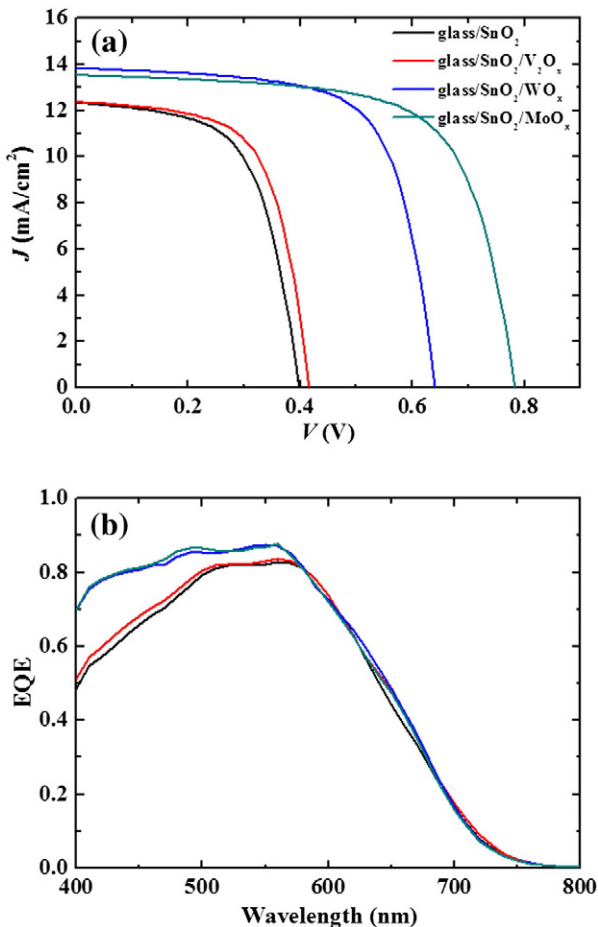


Fig. 1. Device performances for solar cells with different TMO window layer materials (a) photo  $J$ - $V$  and (b) EQE.

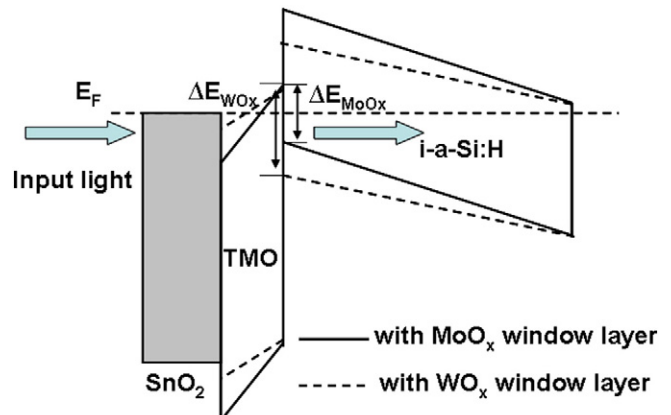


Fig. 2. Band diagram of SnO<sub>2</sub>/TMO/ $i$ - $a$ -Si:H/ $n$ - $a$ -Si structure.

Download English Version:

<https://daneshyari.com/en/article/8035257>

Download Persian Version:

<https://daneshyari.com/article/8035257>

[Daneshyari.com](https://daneshyari.com)